Mavacamten stabilizes a folded-back sequestered super-relaxed state of β-cardiac myosin

Robert L. Anderson[1,a], Darshan V. Trivedi[2,3,a], Saswata S. Sarkar[2,a], Marcus Henze[1], Weikang Ma[5,] Henry Gong[5], Christopher S. Rogers[6], Fiona L. Wong[1], Makenna Morck[2], Kathleen M. Ruppel[2,3,4], Thomas C. Irving[5], Roger Cooke[7], Eric M. Green[1,b,c] and James A. Spudich[2,3,b,c]

[1]MyoKardia Inc., South San Francisco, CA 94080

[2]Department of Biochemistry, Stanford University School of Medicine, Stanford, CA 94305.

[3]Stanford Cardiovascular Institute, Stanford University School of Medicine, Stanford, CA 94305.

[4]Department of Pediatrics (Cardiology), Stanford University School of Medicine, Stanford, CA 94305.

[5]BioCAT, Department of Biological Sciences, Illinois Institute of Technology, Chicago, IL 60616

[6]Exemplar Genetics, Sioux Center, Iowa 51250

[7]Department of Biochemistry, University of California San Francisco, San Francisco, CA 94158

[a] R.L.A., D.V.T. and S.S.S. contributed equally to this work

[b] E.M.G. and J.A.S. contributed equally to this work.

[c] To whom correspondence may be addressed. Email: jspudich@stanford.edu or egreen@myokardia.com

Abstract:

Mutations in β-cardiac myosin, the predominant motor protein for human heart contraction, can alter power output and cause cardiomyopathy. Previous studies suggest that myosin function can be regulated by entering a super-relaxed state (SRX) with very slow ATP hydrolysis, but the structural determinants of this state are uncertain. Using a combination of biochemical approaches with electron microscopy and X-ray fiber diffraction, we show that the SRX corresponds to a folded-back state of myosin with increased ordering of heads around the thick filament backbone. The small molecule mavacamten induces this conformation, while mutations causing HCM destabilize it. These findings provide a structural basis for an important mode of regulation of cardiac myosin with implications for the pathogenesis of cardiomyopathy and potential therapeutic development.

Introduction:

Muscle myosin is a hexamer consisting of two myosin heavy chains and two sets of light chains, the essential light chain (ELC) and the regulatory light chain (RLC). The myosin molecule can be divided into two parts, heavy meromyosin (HMM), which consists of two globular heads and the first ~40% of the coiled-coil tail, and light meromyosin (LMM), which consists of the C-terminal ~60% of the coiled-coil tail. LMM self assembles creating the shaft of the myosin thick filament found in sarcomeres of the muscle. HMM can be further divided into Subfragment 1 (S1), which is the globular head of the myosin that serves as the motor domain (*1*), and subfragment 2 (S2). S1 houses the ATP and actin binding sites followed by an essential light chain (ELC) and regulatory light chain (RLC) bound α-helix (lever arm) (Fig. 1A). S1 heads are arranged on the thick filament backbone in muscle in a helical or quasi-helical fashion. There is a 14.3-nm vertical spacing between two adjacent myosin molecules on the filament with a true repeat of 42.9 nm.

Importantly, intramolecular interactions favoring a folded state of myosin (Fig. 1B) have been observed in both purified myosin preparations (*2-6*) and in myosin thick filaments isolated from muscle (*7-10*). Named the interacting-heads motif (IHM) (*9*), this structure has been proposed to be related to a super-relaxed state (SRX) of muscle, defined as a state that has a much reduced basal ATPase rate of ~ 0.003 s^{-1} (*11*). The SRX was initially discovered in rabbit skeletal muscle and thereafter also seen in rabbit cardiac, tarantula exo-skeletal and mouse and human cardiac fibers (*12-15*). An appealing hypothesis is that the SRX state is related to the IHM myosin state where the myosin S1 heads are interacting with one another and folded back onto their own coiled-coil S2 tail (*13, 16-19*). Since the SRX state has only been described in fibers, it is possible that other sarcomeric proteins in the vicinity of the myosin are essential for establishing this state. There have been no studies that directly demonstrate a structural corollary of the SRX state with purified sysems. Here we demonstrate biochemically that a decrease of basal ATPase to the levels seen in the SRX in fibers can be observed with purified human β-cardiac myosin alone.

Hypertrophic cardiomyopathy (HCM) is an autosomal dominant inherited disease of heart muscle (*20-22*) characterized by hyper-contractility and subsequent hypertrophy of the ventricular walls. Systolic performance of the heart is preserved or even increased, but relaxation

capacity is diminished. Patients with HCM are at increased risk of heart failure, atrial fibrillation and stroke, and sudden cardiac death. Current pharmacological management options are not disease specific and do not address the underlying HCM disease mechanism. It has been hypothesized that a small molecule that binds directly to myosin and normalizes the hyper-contractility of the sarcomere may interrupt the development of downstream pathology (such as hypertrophy, fibrosis and clinical complications) seen in this disease (*23*). Mavacamten (formerly MYK-461; MyoKardia Inc., South San Francisco, CA) is an oral allosteric modulator of cardiac myosin and causes dose-dependent reductions in left ventricular contractility in healthy volunteers and HCM patients (*24*). This investigational drug is in phase 2 clinical trials and is the first in line of potential new HCM therapeutic agents that act directly by interacting with the human β-cardiac myosin and normalizing its power output. Mavacamten was identified in a screen for actin-activated myosin ATPase inhibitors, and it lengthens the total cycle time (t_c) of the ATPase cycle (*25*). This results in a reduction of the duty ratio (t_s/t_c) and therefore of the ensemble force, since $F_{ens} = f_{int} \cdot N_a \cdot$ duty ratio, where f_{int} is the intrinsic force of a myosin molecule and N_a is the total number of myosin heads in the sarcomere that are functionally accessible for interaction with actin. Here we show that mavacamten also reduces N_a by stabilizing the heads in a folded IHM state with a very slow release of bound nucleotide, an SRX-IHM state.

The first HCM-causing mutation in β-cardiac myosin to be identified was R403Q (*20*). As with other HCM mutations, the R403Q mutation results in hyper-contractility of the muscle (*26, 27*). We provide evidence here that the R403Q mutation results in a shift in the equilibrium between the open and closed structures of myosin (Fig. 1B) to the open state, resulting in more heads available for interaction with actin and the hyper-contractility seen clinically. We see a similar phenotype in human cardiac samples with the HCM-causing R663H mutation. We further demonstrate that mavacamten reverses this destabilization of IHM caused by these mutations.

Results:

Purified human ß-cardiac myosin containing the proximal S2 portion of its coiled-coil tail is in an ionic-strength dependent super-relaxed state.

To test the hypothesis that the SRX observed in muscle fibers is related to the folded-back IHM of purified myosin we compared the kinetics of myosin's basal ATPase cycle for three purified human ß-cardiac myosin constructs: 25-hep HMM (two-headed with first 25-heptads of proximal S2), 2-hep HMM (two-headed with first 2-heptads of proximal S2) and short S1 (sS1; single-headed with no S2, and truncated immediately after the ELC binding domain, Fig. 1A). The basal ATPase rates of the three constructs were all within the range of 0.01 to 0.03 s^{-1} (Fig. S1), consistent with high levels of actin-activation of these human ß-cardiac myosin constructs (about 100-fold activation by actin (*28, 29*). SRX is defined as a rate of nucleotide release from the myosin head that is even slower, about 0.003 s^{-1} (*11*).

To test the percentage of heads in the SRX for the three constructs we adapted the single nucleotide-turnover assay, which is typically measured in a stopped-flow apparatus, to a plate-based measurement. The slow rates of normal myosin basal ATPase and the SRX-based nucleotide release makes them amenable to a plate-based measurement. Moreover, owing to the difficulties in expressing high amounts of human cardiac proteins, the plate-based assay is an apt

choice for this kind of experiment. This assay measured the fluorescent nucleotide release rates by loading the myosin heads with mant-ATP and then chasing with excess unlabeled ATP, as had been done in skinned fibers previously (*11*). As the mant-nucleotide is released from the myosin, its fluorescence decreases (*11*).

The decay rate of mant-nucleotide fluorescence for 25-hep HMM was fit well by two exponential rate constants, one representing a basal ATPase rate of heads in a presumed open state (disordered relaxed state, DRX) of ~0.03 s^{-1} and the other representing an SRX rate of ~0.003 s^{-1} (Fig. 2A). In 100 mM potassium acetate (KAc), the amplitudes were 74 ± 2% basal rate and 26 ± 2% SRX rate (Fig. 2B). This SRX level observed for the 25-hep HMM did not vary significantly from preparation to preparation, and may represent myosin heads that are folded back onto their own proximal S2 tail. Consistent with this hypothesis, the fraction of myosin heads in the SRX increased from 26 ± 2% to 42 ± 2% ($p<0.05$) when the KAc was decreased from 100 mM to 25 mM. The SRX further increased from 26 ± 2% to 59 ± 7% ($p<0.05$) when the salt was decreased from 100 mM to 5 mM KAc (Fig. 2B). This would be expected since the IHM structure is thought to be held together largely by charge-charge interactions (*9, 29-32*). The amplitudes of the fast (74 ± 2%) and slow phases (26 ± 2%) observed with the human ß-cardiac 25-hep HMM at 100 mM KAc match closely with the amplitudes observed in SRX experiments done with rabbit cardiac fibers (~70% fast and ~30% slow at 120 mM KAc)(*13*).

In contrast to the 25-hep construct, the 2-hep HMM and sS1, which do not contain the proximal S2 tail, showed < 20% SRX (Fig. 2C-F), regardless of salt concentration ($p > 0.05$ for 2-hep HMM and sS1 salt dependence). Unlike the values seen for 25-hep HMM, the percentage of SRX seen for 2-hep HMM and sS1 were variable, ranging between 0-20% of the population. To ensure that we were not missing any fast phase in our plate-based measurement, we performed the similar measurement with sS1 in a stopped-flow apparatus. The rates and amplitudes obtained were very similar to our plate-based measurements (Fig. S2).

These results suggest that purified myosin can adopt a biochemical SRX that is stabilized by the S2 tail and by low ionic strength conditions that favor electrostatic interactions. These are the first results that directly link, using purified human ß-cardiac myosin, the IHM structural state with the biochemical SRX.

The cardiac myosin inhibitor mavacamten stabilizes the SRX-IHM of purified human ß-cardiac myosin

Using the mant-nucleotide release rates as a measure of the level of SRX in the population, we examined whether the cardiac myosin inhibitor mavacamten has any effect on the distribution of ATPase states in the population of purified human ß-cardiac myosin constructs. While mavacamten was selected on the basis that it inhibits the actin-activated activity of sS1 (*25*), we found that it has a profound effect on stabilizing the SRX. Mavacamten induced a 20-fold reduction in the basal ATPase rate of the 25-hep HMM (Fig. S1A). In the single-nucleotide turnover assay, in the presence of 10 µM mavacamten, the mant-nucleotide release rates from 25-hep HMM at 25 mM KAc were fit well by a single exponential with a rate constant reflecting the SRX. At both 25 mM KAc (Fig 3A,B) and 100 mM KAc (Fig. S3), essentially ~100% of the myosin heads were in the SRX in the presence of mavacamten. In absence of mavacamten, the

fraction of 25-hep HMM in the SRX was ~42% at 25 mM KAc (Fig. 2B) and ~26% at 100 mM KAc (Fig 2B).

The effect of mavacamten on 2-hep HMM was less pronounced (Fig. 3C,D), consistent with a role for the proximal S2 in stabilizing the SRX. However, 40-50% SRX is observed in the presence of mavacamten suggesting that either the heads can interact with one another to some extent in the absence of proximal S2 or mavacamten reduces the ATPase of some of the individual heads to SRX levels. Reduction of the actin-activated ATPase activity of sS1 by mavacamten has been previously demonstrated (*25*), and Fig. 3E,F shows that some level of a reduced basal myosin ATPase rate of ~0.003 s^{-1} can be obtained with sS1 alone. Indeed, mavacamten does reduce the basal myosin ATPase of the 2-hep and sS1 constructs (Fig. S1B, C).

We used electron microscopy to verify that the SRX observed with 25-hep HMM corresponds to folded-back (closed) heads. Fig. 3G shows representative images of closed IHM structures (top panels) and open structures (lower panels). After coupling the 25-hep HMM to a mavacamten analog containing a photoactivatable crosslinker, folded-back IHM structures dominated the images, while the reverse was true in the absence of the mavacamten derivative (DMSO control) (Fig. 3H). Less than 20% of the myosin molecules were in a closed IHM state in the absence of mavacamten and ~60% were in a closed IHM state in the presence of mavacamten (Fig. 3H). These results more firmly link the IHM structural state with the SRX.

The cardiac myosin inhibitor mavacamten stabilizes the SRX-IHM of porcine and human cardiac muscle fibers

To examine whether the effects of mavacamten on purified myosin translate to an increase in the level of SRX in cardiac fibers, we carried out mant-nucleotide release analyses on skinned fibers from relaxed minipig cardiac muscle. Mavacamten increased the percentage of the SRX in the porcine fibers from 26 ± 2% to 39 ± 4% ($p<0.05$, Fig. 4A,B). There is a corresponding decrease in tension measured in skinned porcine cardiac muscle fibers exposed to mavacamten from 14.4 ± 0.7 mN/mm^2 to 6.6 ± 0.7 mN/mm^2 (pCa 5.8, $p < 0.05$, Fig 4C).

A similar mavacamten-mediated SRX stabilization effect was also observed for wild type (WT) human cardiac fibers. Mavacamten increased the SRX in the human fibers from 24 ± 2% to 45 ± 2% ($p<0.05$, Fig. 4D,E). The smaller effect on the fibers compared to the purified 25-hep protein could reflect a role for other components of the intact sarcomere in regulating the SRX population, or accessibility issues of mavacamten to the myosin in the skinned fibers. The ~25% SRX we see in the fibers without mavacamten treatment at 120 mM KAc is consistent with our 25-hep HMM purified protein data at 100 mM KAc (Fig. S3B).

To examine the spatial organization of the myosin heads we used low-angle X-ray diffraction of porcine cardiac muscle fibers, which reveals information about the degree of order of the myosin heads along the myosin thick filaments as well as their proximity to the thin actin filaments. A representative low-angle X-ray diffraction image of a porcine cardiac muscle fiber shows the typical helical diffraction pattern known for striated muscle (Fig. 5).

Mavacamten causes a dramatic ordering of myosin heads along the backbone of the thick filaments as observed by the substantial increase in the myosin-based helical layer line reflections for both relaxed (Fig. 5A vs B, arrows) and contracting (Fig. 5F vs G, arrows) porcine muscle fibers. The first myosin layer line (MLL1) intensity at 43 nm (Fig. 5B,G white arrows) increased about 40% with mavacamten treatment ($MLL1_{+mava}/MLL1_{-mava} = 1.37 \pm 0.13$). If we assume that only myosin heads in the SRX give rise to layer lines, a 40% MLL1 intensity increase would imply 17 ± 6% more heads in the SRX, consistent with the fluorescence decay data shown in Fig. 4A,B. A prominent reflection is the M3 reflection on the meridian, which reports on the 14.3-nm repeat of the myosin heads along the longitudinal shaft of the thick filament in the relaxed state (Fig. 5C). The higher the intensity of this reflection, the more ordered are the heads along this 14.3-nm repeat. When the diffraction pattern of the relaxed muscle in the absence of mavacamten (Fig. 5A) is subtracted from the diffraction pattern in the presence of mavacamten (Fig. 5B), the difference (Fig. 5C) shows that the intensity of the M3 reflection is significantly increased by addition of mavacamten ($p < 0.05$). This is quantified in Fig. 5D where the results from 13 fibers are shown. An even more dramatic increase is seen in the M3 reflection when mavacamten is added to contracting fibers ($p < 0.05$, Fig. 5F-I). Thus, for both relaxed and contracting fibers, mavacamten increases the helical order of myosin heads on the thick filament backbone.

The 1,1 and 1,0 reflections on the equator provide information on the number of myosin heads that have moved away from the myosin thick filaments toward the actin thin filaments. The 1,1 lattice planes include the actin filament densities, while the 1,0 lattice planes include only the myosin thick filament densities. Thus an increase in the intensity of the 1,0 reflection shows that more myosin heads have been sequestered near the shaft of the thick filaments, and the $I_{1,1}/I_{1,0}$ intensity ratio is reduced. As can be seen in Fig. 5C and H, mavacamten causes an increase in the 1,0 reflection intensity. Furthermore, Fig. 5E and J show that the $I_{1,1}/I_{1,0}$ intensity ratio is reduced ($p < 0.05$) by mavacamten in both relaxing and contracting conditions, suggesting that it causes more heads to become sequestered against the LMM backbone of the myosin thick filament.

These structural results, combined with the studies with purified human ß-cardiac myosin described above, suggest that mavacamten shifts the open-closed state equilibrium toward the closed SRX-IHM state, which in muscle fibers is more ordered near and along the backbone of the myosin thick filament.

The hypertrophic cardiomyopathy mutation R403Q reduces the level of SRX in cardiac muscle fibers

To better characterize the effects of mutations that cause HCM on cardiac structure and function, we generated a large animal model of HCM in the Yucatan minipig (Fig. S4 and Methods). We introduced into minipigs the heterozygous *MYH7* R403Q mutation, which has been well-characterized in mice and humans (*20, 33*). When cardiac fibers from the R403Q pigs were compared with those from the WT pigs for SRX levels, strikingly, the R403Q mutation caused a significant decrease in the percentage of SRX in the porcine fibers, from 26 ± 2% to 20 ± 2% ($p<0.05$, compare Fig. 6A,B with Fig. 4A,B). This result supports the hypothesis that myosin HCM mutations cause clinical hyper-contractility by shifting the equilibrium from the closed off-state (SRX-IHM) to the open on-state where the heads are free to interact with actin (*29, 30, 34-36*). Addition of mavacamten to the R403Q fibers returned the percentage of SRX back to the normal WT level (30 ± 5%, $p<0.05$) and also reduced tension from 14.9 ± 0.7 mN/mm^2 to 8.1 ±

0.6 mN/mm^2 (pCa 5.8, $p < 0.05$, Fig. 6C). The physiologically-relevant pCa range for tension development in the heart is from ~10^{-7} M Ca^{2+} to ~10^{-6} M Ca^{2+} (red shaded area, Fig. S5) (*37*), where the R403Q mutation induces hyper-contractility and mavacamten reduces it towards normal (light blue to dark blue shaded area, Fig. S5).

Treatment of R403Q skinned porcine fibers with mavacamten caused an increase in ordering of myosin heads along the backbone of the myosin thick filament, as judged by an increase in the myosin-based helical layer lines (black arrows) and the intensity of the M3 reflection (white arrow) (Fig. 6E), consistent with a shift in equilibrium toward the myosin SRX-IHM off-state (Fig. 6D,E). This mavacamten-dependent increase in the intensity of the M3 reflection was observed under relaxing conditions. Such an intensity change was difficult to quantify for the R403Q fibers under contracting conditions. Mavacamten also caused a significant decrease in the $I_{1,1}/I_{1,0}$ intensity ratio of the R403Q fibers ($p < 0.05$) (Fig. 6E-G), further supporting a shift in equilibrium toward the myosin SRX-IHM off-state more closely associated with the backbone of the myosin thick filament. This effect was quantified for the R403Q fibers under both relaxing and contracting conditions.

We also studied the properties of the SRX in a known human pathogenic HCM mutation, *MYH7* R663H with fibers isolated from human cardiac tissue. We found that the R663H mutation caused a significant decrease in the percentage of SRX from 24 ± 2% (WT human cardiac tissue) to 18 ± 2% (R663H human cardiac tissue) ($p<0.05$), and that the addition of mavacamten to these fibers restored the SRX levels back to 37 ± 6% ($p<0.05$), which is similar to the WT level (Fig. 6H,I). These changes are similar to those observed with the R403Q porcine samples and suggest that HCM mutations in myosin destabilize SRX in both pigs and humans.

Discussion:

Over the past five decades our understanding of muscle physiology, biochemistry and biophysics has greatly advanced. While not complete, we have a good understanding of how many of the most important sarcomeric proteins function and their roles in muscle contractility. Now focus is shifting to understanding the molecular basis of disease states of these proteins and modern therapeutic approaches that can be applied to them. This study focuses on HCM mutations that cause hyper-contractility of the heart and a small molecule, mavacamten, which resets this hyper-contractility to normal.

Recent studies using human ß-cardiac myosin support the view that many, if not most, myosin missense HCM mutations cause the hyper-contractility observed clinically by shifting an equilibrium between a sequestered off-state of myosin heads to their on-state now able to interact with actin (*28-30, 34, 36, 38-40*). The majority of these mutations are highly localized to three surfaces of the myosin molecule: the converter domain (*30, 39*) (Fig. 1A), a relatively flat surface named the myosin mesa (*34*) (Fig. 1B), and the proximal part of S2 that interacts with the S1 heads in the IHM (*28-30, 36, 38-40*) (Fig. 1B).

The realization that the myosin mesa of the two S1 heads in the IHM are in fact cradling the proximal S2 (Fig. 1B) was striking (*28, 29*). Moreover, the mesa is highly enriched in HCM mutations in positively-charged Arg residues (*34*), whereas the proximal S2 is highly enriched in HCM mutations in negatively-charged Glu and Asp residues (*39*). Furthermore, the converter

HCM mutations are all in a position to potentially disrupt the IHM at a primary head-head interaction site (PHHIS) involving a particular surface of the 'blocked head' of the IHM and the converter of the 'free head'(*29, 30, 40*). We conclude that it is a reasonable hypothesis that myosin missense HCM mutations weaken the SRX-IHM state, resulting in more functionally accessible myosin heads for actin interaction, thus causing the hyper-contractility observed for HCM clinically.

In support of this model, several positively-charged mesa HCM residues, R249Q, H251N, and R453C, significantly weaken the binding of proximal S2 to sS1 in biochemical experiments with purified myosin fragments, and D906G on the proximal S2 that is near the interface with the mesa in the human ß-cardiac myosin folded-back homology models has the same effect (*28, 29*). Interestingly, R403Q has no effect on the affinity of S2 for sS1 (*29*), while here we show that it reduces the amount of SRX in muscle fibers.

So what is R403Q doing at the molecular level? R403Q is in a unique position on the myosin surface, residing at the tip of a pyramid formed by three interacting faces, the actin binding face, the mesa, and the PHHIS (*29, 36*). R403Q does not seem to have a significant effect on actin interaction (*41*), but it could be weakening the complex by weakening the blocked head PHHIS interaction with the free head converter (*29, 36*). Arg403 is also in a position to possibly bind to part of MyBP-C (*29, 36*) and the R403Q mutation may weaken a MyBP-C-SRX complex, and in this way shift the equilibrium away from the SRX in fibers.

Similarly, it is not known which of these various interactions the mesa HCM mutation R663H is affecting, but we show here that it reduces the level of SRX in fibers. Biochemical experiments involving the effects of R403Q and R663H on the interactions between these human ß-cardiac sarcomeric protein players will be necessary to elucidate the molecular mechanism of how these mutations reduce the SRX in the fiber.

The small molecule mavacamten, a cardiac inhibitor in phase 2 clinical trials, decreases contractility and suppresses the development of hypertrophy and fibrosis in HCM mouse models (*25*). How is this molecule affecting the detailed structure of the myosin active site? The presence of ATP or ADP.Pi analogs in the active site of myosin causes the switch elements to adopt a closed state, which in-turn has been inferred to stabilize the helical order of the thick filament (*42-44*). Blebbistatin, a small molecule ATPase inhibitor, stabilizes a closed switch-2 state and has also been shown by electron microscopy (*45*) and fluorescence-based studies (*46*) to stabilize the IHM state of myosin. Conversely, omecamtiv mecarbil (OM), a cardiac activator in phase 3 clinical trials, has been shown to stabilize the open state of myosin on the cardiac thick filament (*46*). Along similar lines, mavacamten has been previously shown to reduce the basal release rates of ADP and Pi (*47*), possibly by holding the switch elements in a closed state, which ultimately stabilizes the myosin heads in the SRX-IHM state. The high-resolution detailed structural basis of formation of the SRX-IHM state is an intriguing, open question in the field. It is crucial now to obtain a high-resolution crystallographic or cryo-EM structure of the SRX-IHM.

We provide here the first evidence at the biochemical level that the cardiac SRX can occur with nothing more than an HMM-like molecule containing two S1 heads and the proximal part of the coiled-coil tail, and that the level of SRX decreases with increasing ionic strength, consistent with many charge-charge interactions stabilizing the IHM. Our work demonstrates that the tail region of myosin is necessary to fully stabilize its SRX conformation. Our 2-hep HMM,

however, shows SRX behavior without the proximal tail, which may indicate that the PHHIS-converter association (*29, 36, 40*), as well as other important interactions (*30*) may be enough to hold the heads in a less stable SRX. But even sS1 shows a 15-20% population of SRX, which increases to ~50% SRX in the presence of mavacamten. It is important to note that myosin molecules in solution in any nucleotide state are likely to exist in a number of closely-related conformational states in equilibrium. We think it likely, therefore, that a small part of the population of independent sS1 molecules in solution exist in a conformation that is similar to that stabilized in the IHM structure, and the binding of mavacamten shifts the equilibrium of sS1 heads in solution toward the structure of the heads in the SRX-IHM state. In the context of HMM, this conformation favors the interactions with the proximal S2 and other head-head interactions that define the SRX-IHM. Thus, strictly speaking, the SRX is not the IHM state directly, but the conformation of the heads that are stabilized by intramolecular interactions in the SRX-IHM. Structural studies will be necessary to assess this possibility further.

The SRX off-state to free head on-state transition of the myosin heads in muscle is thought to be modulated by various factors. One possible factor is the stress sensed by the thick filament as a function of the number of heads that are in the on-state and interacting with actin. This stress-sensing mechanism may be important to maintain the helical order of the myosin heads on the thick filament, and increases in the stress level leads to a destabilization of the SRX-IHM and subsequent opening of the heads (*48-51*). Thus, there is cross-talk between the global thick filament structure and the conformation of the myosin heads in the SRX-IHM. It has been suggested that this tension sensing is likely to explain the Frank-Starling effect (*49, 50*), long debated with regard to its mechanism of action (*52*).

Other factors modulating the SRX off-state to free head on-state transition could be phosphorylation of the regulatory light chain (*29, 36, 53, 54*), and/or phosphorylation of MyBP-C (*29, 36, 55*). There are reported phosphorylation sites on the cardiac ELC as well (*56*), whose possible role in the stabilization of SRX is unknown. A great deal of work needs to be done to determine what factors modulate the the SRX off-state to free head on-state transition.

Our work presents the first structural and biochemical evidence equating IHM to the SRX of myosin and shows that human ß-cardiac myosin HCM mutations in fibers both from a heterozygous piglet and a human heterozygous patient cause a reduction in the SRX. This work opens up avenues for the development of novel therapeutics that specifically target the open-closed equilibrium of the myosin heads. It is conceivable that future cardiac activators can be designed such that they stabilize the open state, while inhibitors like mavacamten stabilize the closed state of the myosin molecule in the thick filament. This forms an innovative basis of modulating cardiac contractility at the molecular level.

References:

1. Y. Y. Toyoshima *et al.*, Myosin subfragment-1 is sufficient to move actin filaments in vitro. *Nature* **328**, 536-539 (1987).
2. T. Wendt, D. Taylor, T. Messier, K. M. Trybus, K. A. Taylor, Visualization of head-head interactions in the inhibited state of smooth muscle myosin. *J Cell Biol* **147**, 1385-1390 (1999).

3. T. Wendt, D. Taylor, K. M. Trybus, K. Taylor, Three-dimensional image reconstruction of dephosphorylated smooth muscle heavy meromyosin reveals asymmetry in the interaction between myosin heads and placement of subfragment 2. *Proc Natl Acad Sci U S A* **98**, 4361-4366 (2001).
4. S. A. Burgess *et al.*, Structures of smooth muscle myosin and heavy meromyosin in the folded, shutdown state. *J Mol Biol* **372**, 1165-1178 (2007).
5. H. S. Jung *et al.*, Role of the tail in the regulated state of myosin 2. *J Mol Biol* **408**, 863-878 (2011).
6. H. S. Jung, S. Komatsu, M. Ikebe, R. Craig, Head-head and head-tail interaction: a general mechanism for switching off myosin II activity in cells. *Mol Biol Cell* **19**, 3234-3242 (2008).
7. J. L. Woodhead *et al.*, Atomic model of a myosin filament in the relaxed state. *Nature* **436**, 1195-1199 (2005).
8. M. E. Zoghbi, J. L. Woodhead, R. L. Moss, R. Craig, Three-dimensional structure of vertebrate cardiac muscle myosin filaments. *Proc Natl Acad Sci U S A* **105**, 2386-2390 (2008).
9. L. Alamo *et al.*, Three-dimensional reconstruction of tarantula myosin filaments suggests how phosphorylation may regulate myosin activity. *J Mol Biol* **384**, 780-797 (2008).
10. H. A. Al-Khayat, R. W. Kensler, J. M. Squire, S. B. Marston, E. P. Morris, Atomic model of the human cardiac muscle myosin filament. *Proc Natl Acad Sci U S A* **110**, 318-323 (2013).
11. J. W. McNamara, A. Li, C. G. Dos Remedios, R. Cooke, The role of super-relaxed myosin in skeletal and cardiac muscle. *Biophys Rev* **7**, 5-14 (2015).
12. M. A. Stewart, K. Franks-Skiba, S. Chen, R. Cooke, Myosin ATP turnover rate is a mechanism involved in thermogenesis in resting skeletal muscle fibers. *Proc Natl Acad Sci U S A* **107**, 430-435 (2010).
13. P. Hooijman, M. A. Stewart, R. Cooke, A new state of cardiac myosin with very slow ATP turnover: a potential cardioprotective mechanism in the heart. *Biophys J* **100**, 1969-1976 (2011).
14. N. Naber, R. Cooke, E. Pate, Slow myosin ATP turnover in the super-relaxed state in tarantula muscle. *J Mol Biol* **411**, 943-950 (2011).
15. J. W. McNamara *et al.*, Ablation of cardiac myosin binding protein-C disrupts the super-relaxed state of myosin in murine cardiomyocytes. *J Mol Cell Cardiol* **94**, 65-71 (2016).
16. R. Cooke, The role of the myosin ATPase activity in adaptive thermogenesis by skeletal muscle. *Biophys Rev* **3**, 33-45 (2011).
17. C. Wilson, N. Naber, E. Pate, R. Cooke, The myosin inhibitor blebbistatin stabilizes the super-relaxed state in skeletal muscle. *Biophys J* **107**, 1637-1646 (2014).
18. L. Alamo *et al.*, Conserved intramolecular interactions maintain myosin interacting-heads motifs explaining tarantula muscle super-relaxed state structural basis. *J Mol Biol*, (2016).
19. L. Nogara *et al.*, Spectroscopic Studies of the Super Relaxed State of Skeletal Muscle. *PLoS One* **11**, e0160100 (2016).

20. A. A. Geisterfer-Lowrance *et al.*, A molecular basis for familial hypertrophic cardiomyopathy: a beta cardiac myosin heavy chain gene missense mutation. *Cell.* **62**, 999-1006. (1990).
21. C. E. Seidman, J. G. Seidman, in *The Metabolic and Molecular Bases of Inherited Disease,* C. R. Scriver *et al.*, Eds. (McGraw-Hill, 2000), pp. 5532-5452.
22. J. G. Seidman, C. E. Seidman, The Genetic Basis for Cardiomyopathy: from Mutation Identification to Mechanistic Paradigms. *Cell* **104**, 557-567 (2001).
23. J. A. Spudich, Hypertrophic and dilated cardiomyopathy: four decades of basic research on muscle lead to potential therapeutic approaches to these devastating genetic diseases. *Biophys J* **106**, 1236-1249 (2014).
24. M. Maron *et al.*, Abstract 16842: Obstructive Hypertrophic Cardiomyopathy: Initial Single Ascending Dose Data in Healthy Volunteers and Patients. *Circulation* **134**, A16842-A16842 (2016).
25. E. M. Green *et al.*, A small-molecule inhibitor of sarcomere contractility suppresses hypertrophic cardiomyopathy in mice. *Science* **351**, 617-621 (2016).
26. W. S. Wilson, J. M. Criley, R. S. Ross, Dynamics of left ventricular emptying in hypertrophic subaortic stenosis. A cineangiographic and hemodynamic study. *Am Heart J* **73**, 4-16 (1967).
27. M. J. Tyska *et al.*, Single-molecule mechanics of R403Q cardiac myosin isolated from the mouse model of familial hypertrophic cardiomyopathy. *Circ Res* **86**, 737-744 (2000).
28. A. S. Adhikari *et al.*, Early-Onset Hypertrophic Cardiomyopathy Mutations Significantly Increase the Velocity, Force, and Actin-Activated ATPase Activity of Human beta-Cardiac Myosin. *Cell Rep* **17**, 2857-2864 (2016).
29. S. Nag *et al.*, The myosin mesa and the basis of hypercontractility caused by hypertrophic cardiomyopathy mutations. *Nat Struct Mol Biol*, (2017).
30. L. Alamo *et al.*, Effects of myosin variants on interacting-heads motif explain distinct hypertrophic and dilated cardiomyopathy phenotypes. *Elife* **6**, (2017).
31. J. R. Moore, L. Leinwand, D. M. Warshaw, Understanding Cardiomyopathy Phenotypes Based on the Functional Impact of Mutations in the Myosin Motor. *Circulation Research* **111**, 375-385 (2012).
32. W. Blankenfeldt, N. H. Thoma, J. S. Wray, M. Gautel, I. Schlichting, Crystal structures of human cardiac beta-myosin II S2-Delta provide insight into the functional role of the S2 subfragment. *Proc Natl Acad Sci U S A* **103**, 17713-17717 (2006).
33. A. A. Geisterfer-Lowrance *et al.*, A mouse model of familial hypertrophic cardiomyopathy. *Science* **272**, 731-734 (1996).
34. J. A. Spudich, The myosin mesa and a possible unifying hypothesis for the molecular basis of human hypertrophic cardiomyopathy. *Biochem Soc Trans* **43**, 64-72 (2015).
35. S. Nag *et al.*, Beyond the myosin mesa: a potential unifying hypothesis on the underlying molecular basis of hyper-contractility caused by a majority of hypertrophic cardiomyopathy mutations. *bioRxiv*, (2016).
36. D. V. Trivedi, A. S. Adhikari, S. S. Sarkar, K. M. Ruppel, J. A. Spudich, Hypertrophic cardiomyopathy and the myosin mesa: viewing an old disease in a new light. *Biophys Rev* **10**, 27-48 (2018).

37. M. J. Previs *et al.*, Myosin-binding protein C corrects an intrinsic inhomogeneity in cardiac excitation-contraction coupling. *Sci Adv* **1**, (2015).
38. J. A. Spudich *et al.*, Effects of hypertrophic and dilated cardiomyopathy mutations on power output by human beta-cardiac myosin. *J Exp Biol* **219**, 161-167 (2016).
39. J. R. Homburger *et al.*, Multidimensional structure-function relationships in human beta-cardiac myosin from population-scale genetic variation. *Proc Natl Acad Sci U S A* **113**, 6701-6706 (2016).
40. M. Kawana, S. S. Sarkar, S. Sutton, K. M. Ruppel, J. A. Spudich, Biophysical properties of human beta-cardiac myosin with converter mutations that cause hypertrophic cardiomyopathy. *Sci Adv* **3**, e1601959 (2017).
41. S. Nag *et al.*, Contractility parameters of human beta-cardiac myosin with the hypertrophic cardiomyopathy mutation R403Q show loss of motor function. *Sci Adv* **1**, e1500511 (2015).
42. S. Xu *et al.*, The M.ADP.Pi state is required for helical order in the thick filaments of skeletal muscle. *Biophys J* **77**, 2665-2676 (1999).
43. S. Xu, G. Offer, J. Gu, H. D. White, L. C. Yu, Temperature and ligand dependence of conformation and helical order in myosin filaments. *Biochemistry* **42**, 390-401 (2003).
44. M. E. Zoghbi, J. L. Woodhead, R. Craig, R. Padron, Helical order in tarantula thick filaments requires the "closed" conformation of the myosin head. *J Mol Biol* **342**, 1223-1236 (2004).
45. F. Q. Zhao, R. Padron, R. Craig, Blebbistatin stabilizes the helical order of myosin filaments by promoting the switch 2 closed state. *Biophys J* **95**, 3322-3329 (2008).
46. T. Kampourakis, X. Zhang, Y. B. Sun, M. Irving, Omecamtiv mercabil and blebbistatin modulate cardiac contractility by perturbing the regulatory state of the myosin filament. *J Physiol* **596**, 31-46 (2018).
47. R. F. Kawas *et al.*, A small-molecule modulator of cardiac myosin acts on multiple stages of the myosin chemomechanical cycle. *J Biol Chem* **292**, 16571-16577 (2017).
48. M. Linari *et al.*, Force generation by skeletal muscle is controlled by mechanosensing in myosin filaments. *Nature* **528**, 276-279 (2015).
49. M. Reconditi *et al.*, Myosin filament activation in the heart is tuned to the mechanical task. *Proc Natl Acad Sci U S A* **114**, 3240-3245 (2017).
50. Y. Ait-Mou *et al.*, Titin strain contributes to the Frank-Starling law of the heart by structural rearrangements of both thin- and thick-filament proteins. *Proc Natl Acad Sci U S A* **113**, 2306-2311 (2016).
51. M. Irving, Regulation of Contraction by the Thick Filaments in Skeletal Muscle. *Biophys J* **113**, 2579-2594 (2017).
52. R. J. Solaro, Mechanisms of the Frank-Starling law of the heart: the beat goes on. *Biophys J* **93**, 4095-4096 (2007).
53. T. Kampourakis, M. Irving, Phosphorylation of myosin regulatory light chain controls myosin head conformation in cardiac muscle. *J Mol Cell Cardiol* **85**, 199-206 (2015).
54. T. Kampourakis, Y. B. Sun, M. Irving, Myosin light chain phosphorylation enhances contraction of heart muscle via structural changes in both thick and thin filaments. *Proc Natl Acad Sci U S A* **113**, E3039-3047 (2016).

55. T. Kampourakis, Z. Yan, M. Gautel, Y. B. Sun, I. M., Myosin binding protein-C activates thin filaments and inhibits thick filaments in heart muscle cells. *Proc Natl Acad Sci U S A* **111**, 18763-18768 (2014).
56. W. Huang, D. Szczesna-Cordary, Molecular mechanisms of cardiomyopathy phenotypes associated with myosin light chain mutations. *J Muscle Res Cell Motil* **36**, 433-445 (2015).

Acknowledgements:

The authors thank Dr. Sharlene Day of University of Michigan for providing human R663H and WT tissue samples. We thank Dr. Roger Craig and Dr. Kyoung-Hwan Lee of University of Massachusetts, Worcester for the invaluable training and guidance during initial phases of the electron microscopy work. We also thank John Perrino of the Stanford Microscopy Facility for technical help with the electron microscopy work, and all members of the Spudich lab for discussions. E.M.G and J.A.S. conceived and supervised the research. D.V.T., S.S.S. and M.M. performed biochemical experiments with purified human ß-cardiac myosins and analyzed the data. D.V.T., S.S.S. and K.M.R. expressed and purified the proteins. R.L.A., M.H., W.M., H.G and F.L.W., T.C.I and R.C. performed biochemical and structural experiments on porcine and human skinned fibers and analyzed the data. Figures were prepared by R.L.A., D.V.T., S.S.S., E.M.G. and J.A.S. All authors discussed the data as it evolved and reviewed and edited the paper. This work was funded by NIH grants GM33289 and HL117138 (J.A.S.), and AR062279 (R.C.). D.V.T is supported by a Stanford Lucile Packard CHRI Postdoctoral Award (UL1 TR001085) and an American Heart Association Postdoctoral Fellowship (17POST33411070). The electron microscopy project described was supported, in part, by ARRA Award Number 1S10RR026780-01 from the National Center for Research Resources (NCRR). Its contents are solely the responsibility of the authors and do not necessarily represent the official views of the NCRR or the National Institutes of Health.This research used the Nikon Imaging center, UCSF; and, resources of the Advanced Photon Source, a U.S. Department of Energy (DOE) Office of Science User Facility operated for the DOE Office of Science by Argonne National Laboratory under Contract No. DE-AC02-06CH11357. This project was supported by grant 9 P41 GM103622 from the National Institute of General Medical Sciences of the National Institutes of Health. The content is solely the responsibility of the authors and does not necessarily reflect the official views of the National Institute of General Medical Sciences or the National Institutes of Health (T.C.I.).

Competing interests: J.A.S. is a founder of Cytokinetics and MyoKardia, a biotechnology company developing small molecules that target the sarcomere for the treatment of inherited cardiomyopathies, and a member of their advisory boards. R.L.A., M.H., and F.L.W. are employees of and own shares in MyoKardia. E.M.G. owns shares in MyoKardia. K.M.R. and R.C. are members of the MyoKardia scientific advisory board. The content is solely the responsibility of the authors and does not necessarily represent the official view of the National Institutes of Health.

Supplementary Materials:

Materials and Methods
Fig S1-S5
References

FIGURES:

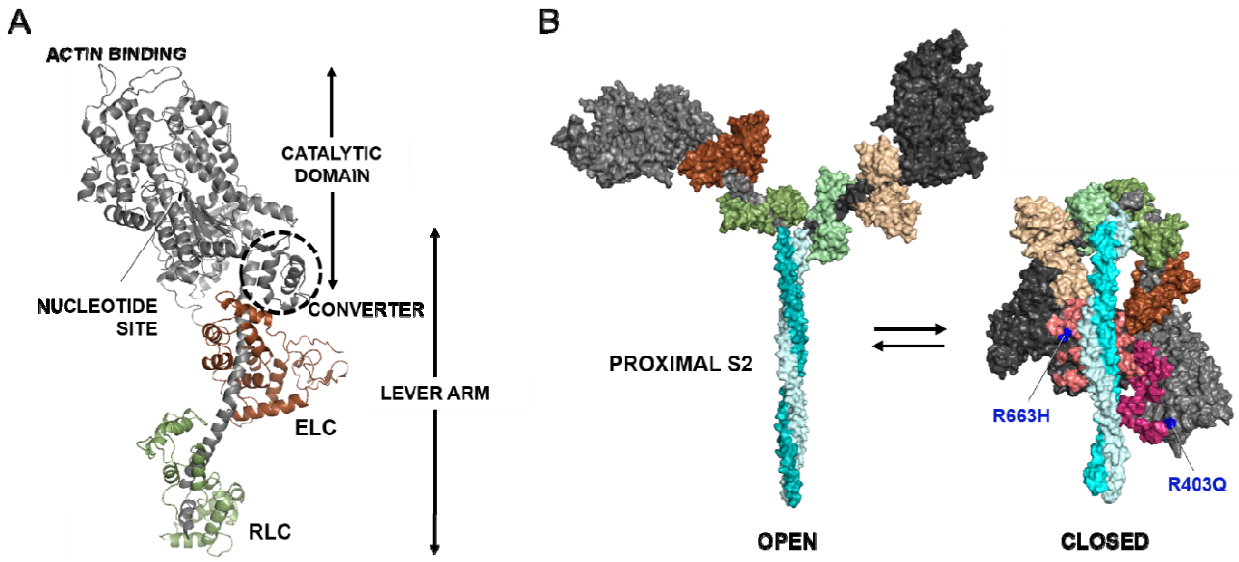

Fig. 1. Human β-cardiac myosin structural models. (A) Pymol homology model of human β-cardiac myosin subfragment 1 (S1) in the pre-stroke state showing its various domains. ELC, essential light chain (brown); RLC, regulatory light chain (green). Modeling was done as described previously (*29, 36*). **(B)** Structural models of the open on-state and the closed IHM off-state of human β-cardiac myosin. The motor domains are black (blocked head) and dark gray (free head), while the ELCs are in shades of brown, and RLCs in shades of green. The positions of R403Q and R663H (blue) are shown in the IHM relative to the mesa residues (*36*) (light pink, blocked head; dark pink, free head). Modeling was done as described previously (*29, 36*).

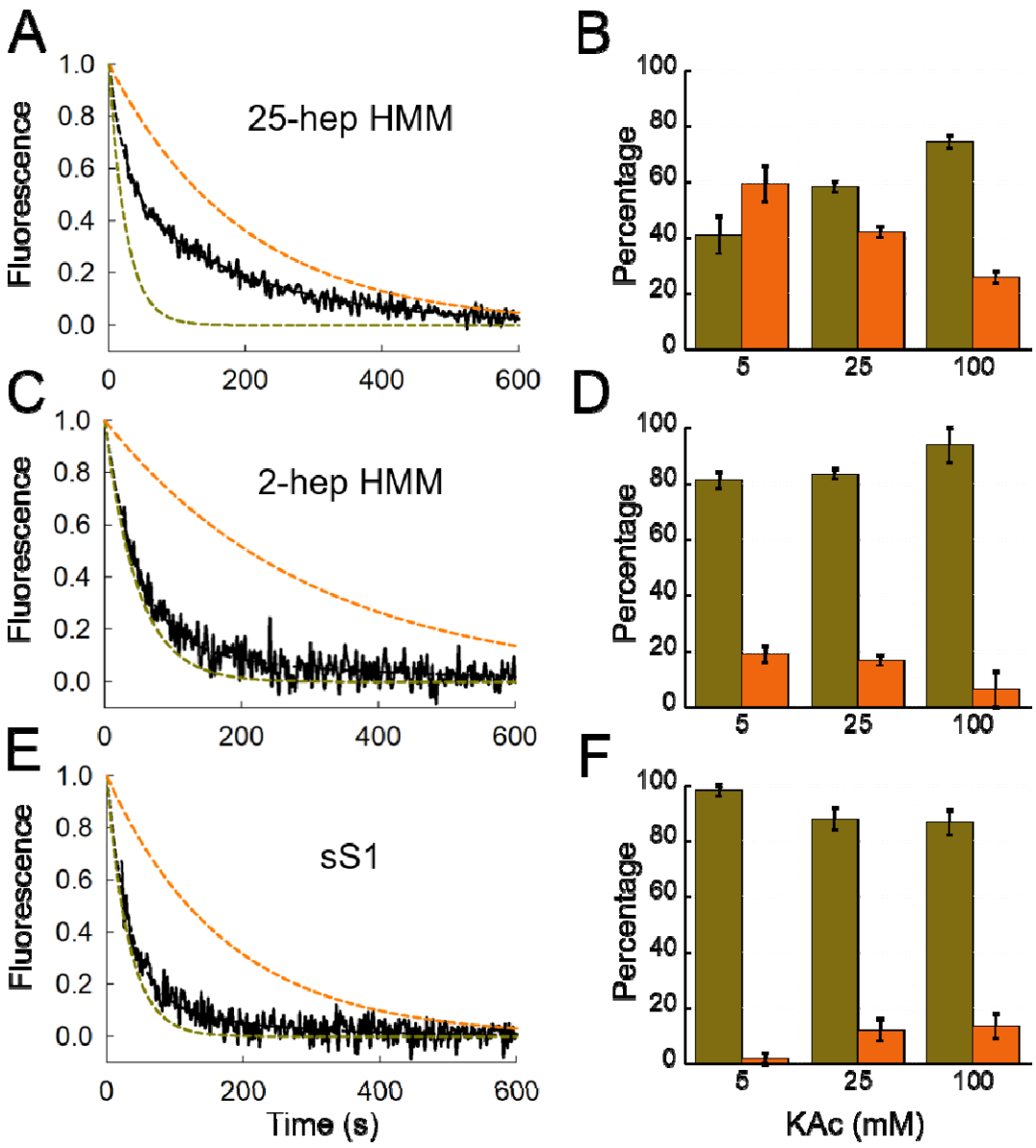

Fig. 2. Mant-nucleotide release rates for purified human ß-cardiac myosin fragments. (A, C, E) Fluorescence decays of mant-nucleotide release from 25-hep HMM, 2-hep HMM and sS1, respectively, in 25 mM KAc. (solid black curves). The simulated single-exponential orange dashed curves are the SRX rate (0.003 - 0.005 s^{-1}) and the simulated single-exponential dashed olive green curves are the DRX rate (0.02 – 0.04 s^{-1}). The simulated orange and olive green dashed curves act as references for the single exponential fits of slow and fast phases, respectively, that derive from fitting the solid black data curves with the best two exponential fits. Thus, the data (black lines) were fit with a combination of these two single exponentials. **(B, D, F)** Percentage of myosin heads in the SRX (orange) versus DRX (olive green) states calculated from the amplitudes of the double-exponential fits of the fluorescence decays corresponding to the mant-nucleotide release from the 25-hep HMM, 2-hep HMM and sS1 constructs at various KAc concentrations. Error bars denote s.e.m.

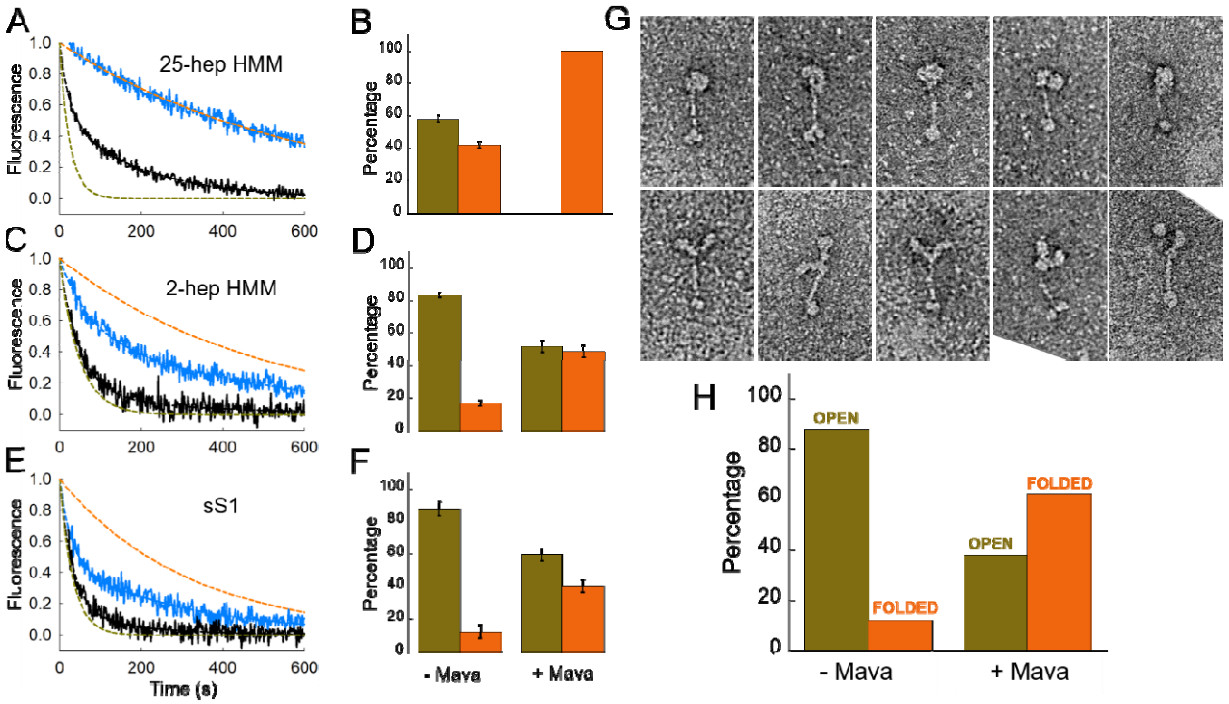

Fig. 3 Mant-nucleotide release rates and percentage folded states for purified human ß-cardiac myosin fragments with and without mavacamten. (A, C, E) Fluorescence decays of mant-nucleotide release from 25-hep HMM, 2-hep HMM and sS1 in 25 mM KAc with (blue curve) and without (black curve) mavacamten. The simulated orange and olive green dashed curves act as references for the single exponential fits of slow and fast phases, respectively, that derive from fitting the solid black data curves with the best two exponential fits. **(B, D, F)** Percentage of myosin heads in the SRX (orange) versus DRX (olive green) states with and without mavacamten calculated from the double-exponential fits of the fluorescence decays corresponding to the mant-nucleotide release from 25-hep HMM, 2-hep HMM and sS1 at 25 mM KAc. **(G)** Panel showing representative single particle negatively-stained electron microscopy images of the open and closed forms of the 25-hep HMM. Both the open and closed molecules have been selected from a sample containing mavacamten crosslinked to 25-hep HMM at 25 mM KAc. **(H)** Percentage of 25-hep HMM molecules in the closed or open form in the presence and absence of mavacamten. Total of 622 and 183 molecules were counted for the with and without mavacamten samples, respectively. Error bars denote s.e.m.

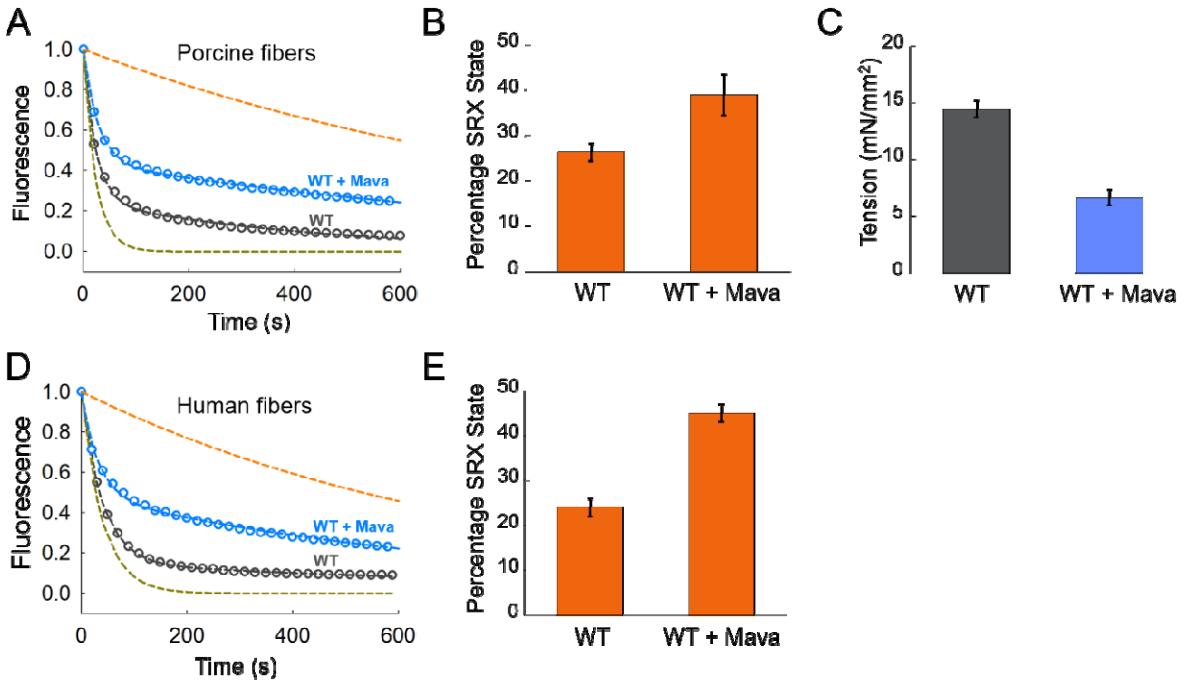

Fig. 4 Effect of mavacamten on wild-type porcine and human cardiac fibers. Blue and dark gray denote experimental conditions with and without mavacamten, respectively. **(A)** SRX measurements with skinned cardiac fibers from wild-type pigs in the presence and absence of mavacamten. The simulated orange and green dashed curves act as references for the single exponential fits of slow and fast phases, respectively, that derive from fitting the solid blue and black data curves with the best two exponential fits. **(B)** Percentage of SRX detected in the porcine cardiac fibers with and without mavacamten. **(C)** Maximum tension measurement in the skinned porcine cardiac fibers in the presence and absence of mavacamten. **(D)** SRX measurements with skinned cardiac fibers from human hearts in the presence and absence of mavacamten**.** **(E)** The percentage of SRX in human cardiac fibers in the presence and absence of mavacamten. Error bars denote s.e.m.

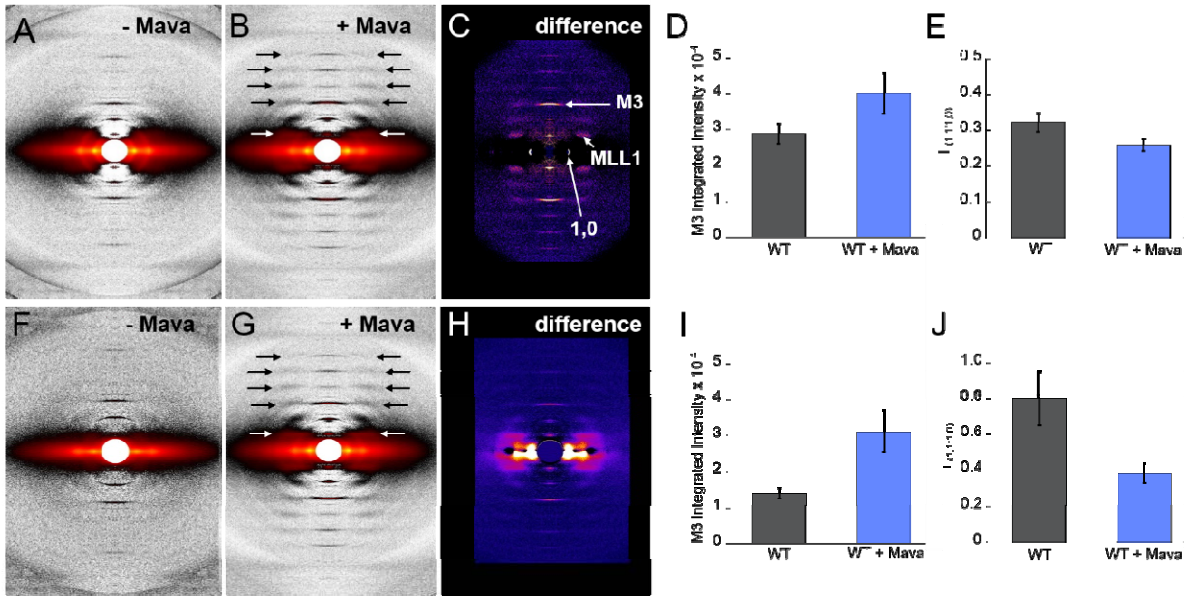

Fig. 5 Effect of mavacamten on ordering of myosin heads onto the thick filaments in wild-type porcine fibers. (A, B, C) Diffraction patterns of wild-type porcine fibers under relaxing conditions (pCa 8) without and with mavacamten and the difference in intensities. **(D)** Mavacamten increases the intensity of the meridional reflection M3 under relaxing conditions. **(E)** Mavacamten decreases the equatorial intensity ratio, $I_{1,1/1,0}$, under relaxing conditions. **(F, G, H)** Diffraction patterns of wild-type porcine fibers under contracting conditions (pCa 4) without and with mavacamten and the difference in intensities. **(I)** Mavacamten increases the intensity of the meridional reflection M3 under contracting conditions. **(J)** Mavacamten decreases the equatorial intensity ratio, $I_{1,1/1,0}$, under contracting conditions. In (D), (E), (I) and (J), blue and dark gray bars denote experimental conditions with and without mavacamten, respectively. Error bars denote s.e.m.

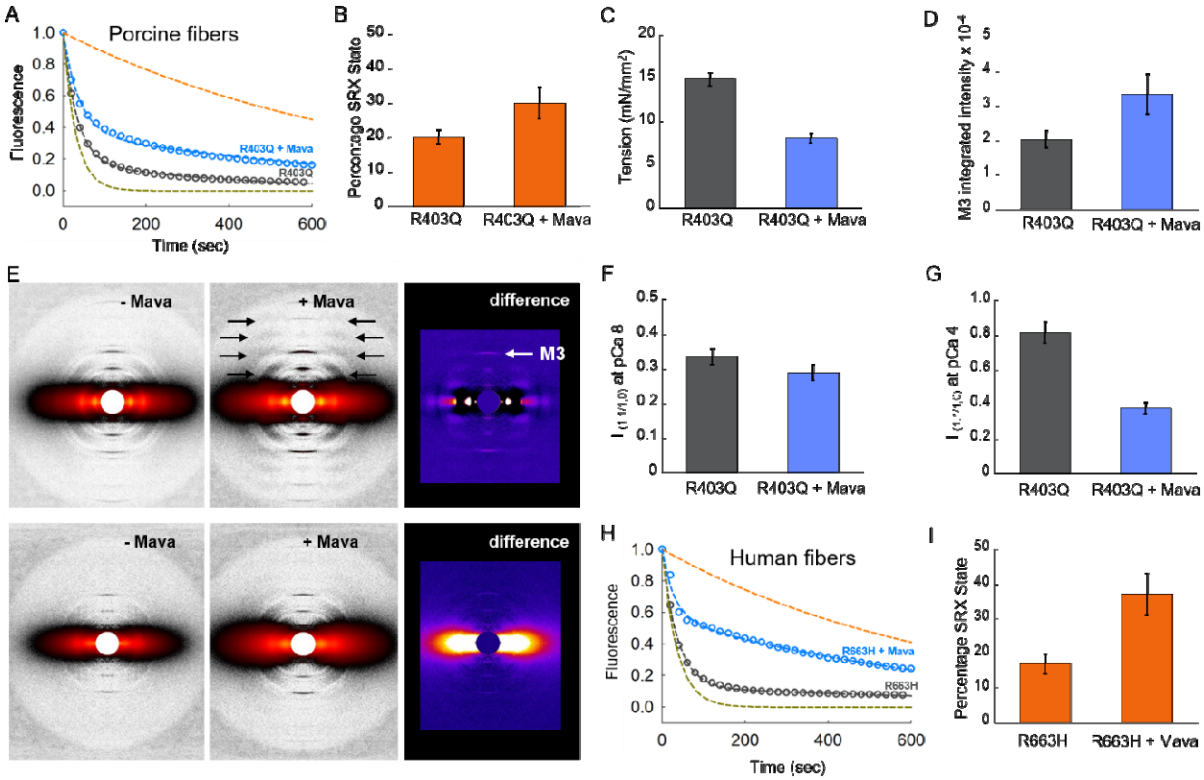

Fig. 6 Mavacamten stabilizes the SRX in porcine and human cardiac fibers carrying HCM mutations. Blue and dark gray denote experimental conditions with and without mavacamten, respectively. **(A)** SRX measurement with skinned cardiac fibers from R403Q pigs in the presence and absence of mavacamten. The green and orange curves are simulated single-exponential fits of fast and slow phase, respectively. **(B)** Percentage of SRX detected in the porcine cardiac fibers with and without mavacamten. **(C)** Maximum tension measurement in the skinned cardiac fibers from R403Q pigs in the presence and absence of mavacamten. **(D)** Mavacamten increases the intensity of the meridional reflection M3 under relaxing conditions. **(E)** Diffraction patterns of R403Q porcine fibers under relaxing conditions (pCa 8) without and with mavacamten and the difference in intensities (top panel). Diffraction patterns of R403Q porcine fibers under contracting conditions (pCa 4) without and with mavacamten and the difference in intensities (bottom panel). **(F)** Mavacamten decreases the equatorial intensity ratio, $I_{1,1/1,0}$, of R403Q porcine fibers under relaxing conditions. **(G)** Mavacamten decreases the equatorial intensity ratio, $I_{1,1/1,0}$, of R403Q porcine fibers under contracting conditions. **(H)** SRX measurements with skinned cardiac fibers from R663H human hearts in the presence and absence of mavacamten. **(I)** The percentage of SRX with and without mavacamten in the R663H human cardiac fibers. Error bars denote s.e.m.